The Astrophysical Journal, 911:65 (12pp), 2021 April 10 https://doi.org/10.3847/1538-4357/abe86a

The Hubble Constant from Infrared Surface Brightness Fluctuation Distances*

John P. Blakeslee[1], Joseph B. Jensen[2], Chung-Pei Ma[3], Peter A. Milne[4], and Jenny E. Greene[5]
[1] Gemini Observatory and NSF's NOIRLab, 950 N. Cherry Avenue, Tucson, AZ 85719, USA; John.Blakeslee@noirlab.edu
[2] Utah Valley University, 800 W. University Parkway, MS 179, Orem, UT 84058, USA
[3] Department of Astronomy, University of California, Berkeley, CA 94720, USA
[4] University of Arizona, Steward Observatory, 933 N. Cherry Avenue, Tucson, AZ 85721, USA
[5] Department of Astrophysical Sciences, Princeton University, Princeton, NJ 08544, USA
Received 2020 December 23; revised 2021 February 9; accepted 2021 February 20; published 2021 April 16

Abstract

We present a measurement of the Hubble constant H_0 from surface brightness fluctuation (SBF) distances for 63 bright, mainly early-type galaxies out to 100 Mpc observed with the WFC3/IR on the Hubble Space Telescope (HST). The sample is drawn from several independent HST imaging programs using the F110W bandpass, with the majority of the galaxies being selected from the MASSIVE survey. The distances reach the Hubble flow with a median statistical uncertainty per measurement of 4%. We construct the Hubble diagram with these IR SBF distances and constrain H_0 using four different treatments of the galaxy velocities. For the SBF zero-point calibration, we use both the existing tie to Cepheid variables, updated for consistency with the latest determination of the distance to the Large Magellanic Cloud from detached eclipsing binaries, and a new tie to the tip of the red giant branch (TRGB) calibrated from the maser distance to NGC 4258. These two SBF calibrations are consistent with each other and with theoretical predictions from stellar population models. From a weighted average of the Cepheid and TRGB calibrations, we derive $H_0 = 73.3 \pm 0.7 \pm 2.4$ km s^{-1} Mpc^{-1}, where the error bars reflect the statistical and systematic uncertainties. This result accords well with recent measurements of H_0 from Type Ia supernovae, time delays in multiply lensed quasars, and water masers. The systematic uncertainty could be reduced to below 2% by calibrating the SBF method with precision TRGB distances for a statistical sample of massive early-type galaxies out to the Virgo cluster measured with the James Webb Space Telescope.

Unified Astronomy Thesaurus concepts: Galaxy distances (590); Distance indicators (394); Cosmological parameters (339); Early-type galaxies (429); Observational cosmology (1146)

1. Introduction

Ever since Cook's first expedition to Tahiti to observe the transit of Venus in 1769 (Cook & Mohr 1771), astronomers have been going to great lengths to measure accurate distances and to corroborate their results through multiple independent routes (see Sawyer Hogg 1947). Distances enable us to convert the observed properties of planets, stars, galaxies, black holes, and cosmic explosions into physical quantities. They reveal the structure of the Local Supercluster, map the peculiar motions, and constrain the present-day expansion rate, parameterized by the Hubble constant H_0. The successful gauging of distances beyond our planet has been the key to understanding the universe.

Increasingly precise distances measured from stellar parallaxes in the Milky Way (e.g., Lindegren et al. 2016; Bailer-Jones et al. 2018), detached eclipsing binaries (DEBs) in the Large Magellanic Cloud (LMC; Pietrzyński et al. 2019), Cepheids in nearby spirals (e.g., Macri et al. 2015; Riess et al. 2020), and a variety of other methods reaching out into the Hubble flow, have progressively pushed down the reported uncertainties on the local expansion rate. For instance, using Type Ia supernovae (SNe Ia) tied to Cepheids, in turn calibrated by a combination of Galactic parallaxes, DEBs in the LMC, and the maser distance to NGC 4258, Riess et al. (2019) find $H_0 = 74.03 \pm 1.42$ km s^{-1} Mpc^{-1}. However, Freedman et al. (2020) conclude $H_0 = 69.6 \pm 0.8 \pm 1.7$ km s^{-1} Mpc^{-1} from a calibration of SNe Ia via the tip of the red giant branch (TRGB), assuming the DEB distance to the LMC. These two studies, which report precise values of H_0 that differ by nearly 2σ, use the same first and third rungs in their distance ladders but differ in the intermediate step (Cepheids versus TRGB).

Also using the LMC-based TRGB method to calibrate SNe Ia but with a different treatment of the extinction for the LMC calibration stars, Yuan et al. (2019) report $H_0 = 72.4 \pm 2.0$ km s^{-1} Mpc^{-1}. Other recent estimates include (omitting units for brevity) $H_0 = 71.1 \pm 1.9$ from the SNe Ia–TRGB method calibrated by the maser distance to NGC 4258 (Reid et al. 2019), 73.3 ± 1.8 from time delays in gravitationally lensed quasars (Wong et al. 2020, see also Harvey 2020), 73.9 ± 3.0 from geometrical distances to galaxies hosting water masers (Pesce et al. 2020), and 75.1 ± 3.0 from the Tully–Fisher method calibrated with Cepheids (Kourkchi et al. 2020b). In general, most techniques for measuring distances in the relatively local universe appear to be converging on a value of $H_0 \approx 73$ km s^{-1} Mpc^{-1}. For a more comprehensive review of the latest results in this rapidly evolving field, see Di Valentino (2021).

In parallel, the exquisitely precise measurements of the cosmic microwave background (CMB) by the Planck mission result in a predicted value of $H_0 = 67.4 \pm 0.5$ km s^{-1} Mpc^{-1},

* Based on observations with the NASA/ESA Hubble Space Telescope, obtained at the Space Telescope Science Institute, which is operated by AURA, Inc., under NASA contract NAS5-26555. These observations come from GO Programs #11711, #11712, #12450, #14219, #14654, #14771, #14804, #15265, #15329.

assuming the standard "lambda cold dark matter" (ΛCDM) cosmology (Planck Collaboration et al. 2020). This lower value of H_0 is not unique to Planck, however. Measurements of baryon acoustic oscillations (BAO) in redshift surveys, which probe the scale of the primordial density fluctuations at later times, in combination with either other CMB data or constraints from big bang nucleosynthesis, imply $H_0 \approx 67 \pm 1$ (Addison et al. 2018; Philcox et al. 2020). In addition, an analysis of the "inverse distance ladder" of SNe Ia calibrated from BAO gives $H_0 = 67.8 \pm 1.3\,\mathrm{km\,s^{-1}\,Mpc^{-1}}$(Macaulay et al. 2019).

A significant discrepancy between the locally measured H_0 and the value implied by primordial density fluctuations within the context of ΛCDM may point to physics beyond the standard paradigm (e.g., Planck Collaboration et al. 2020; Poulin et al. 2019; Knox & Millea 2020). Formally, this discrepancy now exceeds 4σ. Additional evidence for required extensions to ΛCDM comes from the CMB itself, which shows a higher than expected lensing amplitude in its power spectrum (Di Valentino et al. 2020). Alternatively, it could be an indication of unidentified systematics, perhaps lingering coherently in multiple distance estimation methods. For this reason, additional routes to H_0 are worth exploring.

One promising route is the surface brightness fluctuation (SBF) method (Tonry & Schneider 1988; Jensen et al. 1998). The modern SBF method (see the review by Blakeslee 2012) has become an all-purpose precision distance indicator for galaxies that are too distant for TRGB detection, lack young populations that would host Cepheids, and have no known supernovae or the extremely rare water megamasers. Further, unlike Cepheids, SNe Ia, and masers, which all require data spanning multiple epochs, the SBF measurements require only a single observation of sufficient depth, along with color data to provide the stellar population calibration. As a result, the method has been applied widely to study the 3D structure of the nearest galaxy clusters (Mei et al. 2007; Blakeslee et al. 2009; Cantiello et al. 2018a), determine the physical size of the "shadow" (and thus the mass) of the supermassive black hole in M87 (Event Horizon Telescope Collaboration et al. 2019), measure the most precise distance to the host galaxy of the first gravitational wave source with an optical counterpart (GW 170817; Cantiello et al. 2018b), study the satellite systems of nearby galaxies (Carlsten et al. 2019), and confirm the nature of dark-matter-deficient ultradiffuse galaxies (van Dokkum et al. 2018; Cohen et al. 2018; Blakeslee & Cantiello 2018). However, the analysis is not trivial. For an early exposition of the many things that can go wrong with SBF measurements, see Blakeslee et al. (1999a), although most of these problems are avoided with the superb resolution and image stability provided by the Hubble Space Telescope (HST).

The SBF method has been used less frequently to constrain H_0. In some cases, it has served as an intermediate rung on the distance ladder between Cepheids and another method, such as Tully–Fisher, the fundamental plane, or SNe Ia (Tonry et al. 1997; Blakeslee et al. 2002; Khetan et al. 2020). In other cases, the H_0 analysis relied on significant velocity corrections derived from reconstructions of the local gravity field (Blakeslee et al. 1999b; Tonry et al. 2000; Blakeslee et al. 2002). Rarely have SBF studies directly probed the Hubble flow with multiple galaxies—notable exceptions are Jensen et al. (2001) with HST/NICMOS and Biscardi et al. (2008) with HST/ACS (discussed in Section 5 below). However, with the benefit of the Wide-Field Camera 3 Infrared Channel (WFC3/IR) on HST and the calibration provided by Jensen et al. (2015), we can now obtain reliable SBF distances well out into the Hubble flow in a single HST orbit. In this paper, we present the first measurement of H_0 based on a large sample of galaxies with WFC3/IR SBF distances reaching out to 100 Mpc.

2. IR SBF Distances

The SBF method measures the small-scale spatial variance, or "fluctuations," in intensity due to the discrete nature of the stars that comprise a galaxy. Because the fluctuations are dominated by red giant stars in the early-type galaxies we target, the SBF signal is stronger in the near-infrared where these stars are brightest, and the exposure times for measuring SBF distances can be much less than in the optical. The brighter fluctuations, combined with the lower IR background and stable image quality from space, have made it possible to measure robust SBF distances with WFC3/IR out to at least 100 Mpc in one to two HST orbits. As a result, we have been able to amass a large sample of high-quality distances reaching as far as the Coma cluster in a relatively modest amount of time. The galaxy observations come from several different programs but have similar characteristics, as we detail below.

2.1. Observational Data

Our sample comprises 63 galaxies with WFC3/IR imaging in the F110W filter that we have used to measure SBF distances based on the calibration by Jensen et al. (2015). The majority of the observations come from a program (GO-14219) to obtain SBF distances to all galaxies in the MASSIVE survey priority sample (Ma et al. 2014) out to $6000\,\mathrm{km\,s^{-1}}$. MASSIVE is a volume-limited survey to study the structure, stellar populations, internal dynamics, and central black holes of the most massive early-type galaxies within 100 Mpc (e.g., Greene et al. 2015; Veale et al. 2018; Ene et al. 2020; Liepold et al. 2020). Uncertainties in supermassive black hole masses for nearby galaxies are often dominated by distance errors (Kormendy & Ho 2013). Recognizing this, McConnell & Ma (2013) used updated distances for 44 galaxies in their black hole mass compilation, 41 of which were SBF values. Goullaud et al. (2018) present an analysis of the surface brightness profiles for the galaxies targeted in GO-14219.

The $6000\,\mathrm{km\,s^{-1}}$ limit (∼80 Mpc) for the initial WFC3/IR SBF sample was chosen as the point where the typical peculiar velocities of $300\,\mathrm{km\,s^{-1}}$ drop below 5% of the Hubble velocity, meaning that the relative distance error from redshifts is comparable to the expected SBF distance error. In addition, we calculated that in F110W we could reach far enough along the globular cluster luminosity function (GCLF) at this distance to reduce the contamination in the SBF power spectrum to ∼10% in only one orbit. The ability to remove contamination from globular clusters is usually our limiting factor, rather than the signal-to-noise ratio of the SBF signal itself, and this level of detection completeness means that the error in this correction will be $\lesssim$0.03 mag.

Another large fraction of the galaxies in our data set come from a program (GO-14654) to measure SBF distances to host galaxies of well-studied SNe Ia with the goal of investigating possible luminosity differences among subgroups with different ultraviolet colors (e.g., Milne et al. 2013, 2015;

Brown et al. 2017, 2019; Foley et al. 2020). We selected early-type hosts, or in some cases, disk galaxies that appeared to have useful regions for the SBF measurement, based on the imaging data that were available when we were designing the program. These galaxies are naturally less luminous than those in the MASSIVE survey. For three targets in this program that were expected to be near or beyond 80 Mpc, we conservatively obtained two orbits of WFC3/F110W integration to ensure adequate depth along the GCLF.

In a follow-up to GO-14219, program GO-15265 obtained second-band WFC3/UVIS imaging of a subset of the previously targeted MASSIVE galaxies to study the metallicity distributions of their globular clusters. As part of this program, we were also awarded time for single-orbit WFC3/IR F110W imaging of an additional six MASSIVE galaxies beyond our initial 6000 km s^{-1} limit. We have found that we can reliably characterize the GCLFs, and thus correct for their residual contributions to the variance, in these very luminous ellipticals despite the somewhat larger distances. Thus, we have been able to measure the SBF distances for these six galaxies and include them in our sample as well. To these, we add a two-orbit WFC3/F110W observation of the cD galaxy in Coma from another of our programs and single-orbit observations of two galaxies for which we previously published WFC3/F110W SBF distances.

The following list summarizes the HST programs that contributed to the current data set. All of the data were reduced homogeneously by our team.

1. GO-11711: NGC 4874, the cD galaxy in the Coma cluster (PI: J. Blakeslee).
2. GO-12450: NGC 3504 (PI: C. Kochanek), published previously by Nguyen et al. (2020).
3. GO-14219: 35 early-type galaxies selected from MASSIVE Survey (PI: J. Blakeslee).
4. GO-14654: 19 mainly early-type host galaxies of SNe Ia (PI: P. Milne).
5. GO-15265: 6 additional MASSIVE Survey galaxies (PI: J. Blakeslee).
6. GO-14771, GO-14804, GO-15329: NGC 4993, host of the binary neutron star merger that produced GW 170817 (PIs: N. Tanvir, A. Levan, E. Berger), published previously by Cantiello et al. (2018b).

In addition, we also reprocessed the observations from GO-11712 (PI: Blakeslee) that were used by Jensen et al. (2015) to calibrate the WFC3/IR SBF method. This reprocessing was done in order to verify consistency between the calibration and target samples. Although Jensen et al. (2015) presented SBF calibrations for both F110W and F160W, we use only F110W data in the present study and apply the same analysis for all program galaxies. This enables an extremely homogeneous and self-consistent set of distance measurements.

2.2. SBF Measurements

The SBF analysis has been described many times (e.g., Tonry et al. 1990; Jensen et al. 1998; Blakeslee et al. 1999a; Cantiello et al. 2005; Mei et al. 2005). For these HST WFC3/IR data, we follow the procedure documented for the calibration sample by Jensen et al. (2015). Details specific to the present sample of 63 galaxies, including some refinements to the masking process and consistency tests with the calibration sample, are presented in a companion data paper (Jensen et al. 2021, hereafter J21). In brief, we model and subtract the mean galaxy surface brightness, mask contaminating sources (mainly globular clusters and background galaxies) down to some completeness threshold, and measure the Fourier power spectrum of the remaining image. The normalization of the power spectrum on the scale of the point-spread function (PSF) includes contributions from the stellar fluctuations and contaminating sources. We fit and extrapolate the magnitude distribution of the sources and use this to calculate the background variance, which we subtract from the normalization of the PSF component of the power spectrum to get the variance from the stellar fluctuations. These fluctuations are measured in a series of concentric annuli, normalized by the local surface brightness, and converted into the SBF magnitude, labeled $\overline{m}_{110}$ for the F110W bandpass. Applying a calibration for $\overline{M}_{110}$ (see the following section) then gives the distance modulus.

We adopted a photometric zero point of 26.822 AB mag for WFC3/F110W from the STScI website[6] at the time our data were obtained and processed. In December 2020, this value was revised by −0.004 mag based on Bajaj et al. (2020). Although this would change the numerical value of the $\overline{m}_{110}$ measurements tabulated in J21 by a small amount, it would not change our distances, which are referenced to the WFC3/IR SBF calibration of Jensen et al. (2015, see also Cantiello et al. 2018b), who used the former photometric zero point. We correct the photometry for Galactic extinction according to Schlafly & Finkbeiner (2011), using the values provided for individual galaxies by the NASA Extragalactic Database (NED). Following that work, we adopted a 10% uncertainty on the extinction correction and included it in quadrature in our photometric error estimates.

2.3. Color Dependence

The absolute SBF magnitude $\overline{M}$ in a given bandpass depends on stellar population properties such as age, metallicity, initial mass function, alpha-element enhancement, etc. To calibrate this dependence, one generally uses broadband color as a distance-independent proxy for a galaxy's stellar population (e.g., Tonry et al. 1997; Blakeslee et al. 2001; Jensen et al. 2003; Cantiello et al. 2007). Jensen et al. (2015) derived high-quality calibrations of the F110W SBF magnitude $\overline{M}_{110}$ using data for 16 Virgo and Fornax cluster early-type galaxies. For the sake of flexibility, the calibrations were provided using both ACS ($g_{475} - z_{850}$) and WFC3 ($J_{110} - H_{160}$) colors.

Because the broad-baseline optical color is more sensitive to metallicity, the slope of the $\overline{M}_{110}$−($g_{475} - z_{850}$) calibration is shallower and therefore less susceptible to photometric errors; thus, it is the preferred calibration. However, for galaxies with large amounts of foreground extinction (e.g., Cantiello et al. 2018b), or lacking in optical data, the $\overline{M}_{110}$−($J_{110} - H_{160}$) calibration can be used. For the current sample, we adopt the calibration based on optical color for nearly all galaxies, but instead of ACS colors (unavailable for most of the sample), we use colors derived from Pan-STARRS images (Magnier et al. 2020; Waters et al. 2020), with sky estimation and object masking as in Jensen et al. (2015). The photometric transformation of Pan-STARRS ($g - z$) to ACS ($g_{475} - z_{850}$)

[6] https://www.stsci.edu/hst/instrumentation/wfc3/data-analysis/photometric-calibration

is described in detail by J21. We include the scatter in this transformation in our estimate of the color error, which contributes to the uncertainty in the calibrated $\overline{M}_{110}$ for each galaxy.

One galaxy in our sample (ESO 125-G006) lacks Pan-STARRS data; for this, we use 2MASS $(J-H)$ color transformed to $(J_{110}-H_{160})$. As with $(g-z)$, we include the scatter in this transformation in the estimated $\overline{M}_{110}$ error. This galaxy also suffers from the highest amount of Galactic extinction in our sample, 20% higher than the next highest, and more than three times the sample average. Although the color measurement error is amplified by the steeper slope of the $(J-H)$ calibration, the extinction is much lower in the IR, resulting in an error for $\overline{M}_{110}$ only slightly larger than for the rest of the galaxies. The value of H_0 derived from ESO 125-G006 is very close to the best-fit value for the full sample; there is no evidence for any systematic difference resulting from the use of $(J-H)$ for the calibration. Likewise, Cantiello et al. (2018b) found closely consistent distances for the gravitational wave event host NGC 4993 using the two different calibrations; J21 provide further tests illustrating the consistency.

Finally, we note that the dependence of $\overline{M}_{110}$ on galaxy color has some intrinsic scatter due to stellar population effects. For example, galaxies with the same colors may have slightly different $\overline{M}_{110}$ values because age and metallicity are not completely degenerate in their effects on $\overline{M}_{110}$ and broadband color. In the z band, this intrinsic scatter is 0.06 mag for red galaxies (Blakeslee et al. 2009). Although the observed scatter in the $\overline{M}_{110}$ calibration from Jensen et al. (2015) is consistent with measurement error, suggesting a negligible contribution from intrinsic scatter, we conservatively adopt the same 0.06 mag intrinsic scatter for F110W. With this added in quadrature, our median distance modulus error is 0.083 mag, or ∼4% in distance.

2.4. SBF–Cepheid Zero Point

The I-band SBF distance zero point was tied to Cepheids by Tonry et al. (2000) using six spirals that had both SBF and Cepheid distances. This calibration was revised by +0.06 mag by Blakeslee et al. (2002) using the final Key Project Cepheid distances from Freedman et al. (2001), which were based on an LMC distance modulus of 18.50 mag. Additional discussion of this distance zero point, including checks for consistency with HST/ACS SBF distances, is given in Appendix A of Blakeslee et al. (2010). For WFC3/IR, the F110W and F160W SBF zero points were determined by Jensen et al. (2015) using 16 Virgo and Fornax cluster galaxies with previously measured SBF distances by Blakeslee et al. (2009). Cantiello et al. (2018b) revised these zero points by 0.05 ± 0.02 mag following improved PSF characterization resulting from extensive tests with a library of template stars that were used to reanalyze the power spectra of the calibration sample. We use the same set of PSF templates (see J21 for details) and therefore adopt this zero-point shift and its associated scatter.

The above Cepheid calibration assumed a distance modulus of 18.50 mag for the LMC. Based on a sample of 20 DEBs, Pietrzyński et al. (2019) present an improved LMC distance of 49.59 ± 0.55 kpc (combining random and systematic error), or 0.023 ± 0.024 mag less than the value used previously. For consistency with other recent studies (e.g., Riess et al. 2019; Freedman et al. 2019, 2020), we also apply this shift in zero point. The fully revised calibration is presented by J21.

The systematic uncertainty in the $\overline{M}_{110}$ zero point was estimated by Cantiello et al. (2018b) to be 0.10 mag, including contributions of 0.03 mag from the tie between WFC3/IR and optical SBF distances, 0.08 mag from the tie between SBF and Cepheids, and 0.06 mag for the Cepheid zero point, dominated by the uncertainty in the LMC distance. With the improved precision of the revised LMC distance, the Cepheid zero-point error drops to 0.028 mag (Riess et al. 2019), reducing the SBF zero-point uncertainty to 0.09 mag, or 4.2% in distance. This is the current limit of our precision in measuring H_0 using the Cepheid-based SBF calibration alone.

Stellar population models provide confidence in this zero point. Comparisons between SBF predictions for evolved stellar populations and the empirical zero point show agreement in optical bandpasses to better than the 0.09 mag uncertainty (e.g., Blakeslee et al. 2010; Cantiello et al. 2018a; Greco et al. 2021), although there is more discrepancy among models for bluer populations (e.g., Trujillo et al. 2019). The models are less constraining in their predictions for near-IR SBF magnitudes, but they encompass the range of the observations (Jensen et al. 2003, 2015). Empirically, the tie between WFC3/IR and ACS SBF distances is very tight.

2.5. SBF–TRGB Zero Point

Constraints on the zero point can be improved using the TRGB method for red galaxies with well-measured SBF distances. Cohen et al. (2018) show excellent agreement between SBF and TRGB distances for a sample of 12 dwarf galaxies with blue colors observed by HST. However, obtaining an overlapping sample of distances for massive red ellipticals requires reaching the Virgo cluster; there are few TRGB distances for early-type galaxies at this distance. Two exceptions are M60 (NGC 4649; Lee & Jang 2017) and M87 (Bird et al. 2010). There is also a TRGB distance to the massive merger remnant NGC 1316 (Arp 154) in Fornax, which has multiple independent SBF distances (e.g., Blakeslee et al. 2009; Cantiello et al. 2013; Jensen et al. 2015). In the Appendix, we compare the SBF and TRGB distances for these three galaxies using an absolute magnitude for the TRGB itself based on the maser distance to NGC 4258 so that it is fully independent of the LMC-based Cepheid calibration. Excluding the problematic calibrator NGC 1316, we find that the mean offset between the SBF and TRGB distances is -0.01 ± 0.08 mag. In other words, SBF distances would be very slightly longer if calibrated from the TRGB. Including systematic effects, the uncertainty on the TRGB-based SBF zero point becomes 0.10 mag, or 4.6%. Full details are provided in the Appendix.

Clearly, there is no significant difference between the Cepheid-based and TRGB-based SBF zero points. However, the complete independence of the two approaches reduces the final systematic uncertainty on the jointly constrained zero point from >4% for each method independently to 3.1% when combined. Ultimately, we hope to anchor the SBF method using a much larger sample of giant ellipticals with TRGB distances tied to Gaia parallaxes. We return to this prospect in Section 6.

3. Velocity Data

In determining H_0, accurate velocities are equally important as accurate distances. As mentioned above, the majority of our galaxies are massive ellipticals in groups and clusters, including several Abell clusters (see Ma et al. 2014). Many of these

systems have velocity dispersions in excess of 500 km s^{-1}, which would add significant scatter to the Hubble diagram if using individual velocities. We therefore use the group associations and mean group velocities in the CMB frame from Tully (2015), based on the 2MASS Redshift Survey (2MRS; Huchra et al. 2012). The 2MRS is 97.6% complete to magnitude $K_s \leqslant 11.75$ mag over 91% of the sky. The Tully group catalog contains cross-matched identifications to the Crook et al. (2007) catalog that was used by Ma et al. (2014) and based on an earlier version of the 2MRS limited to $K_s \leqslant 11.25$ mag.

For galaxies not in identifiable groups, we use the 2MRS velocity data directly. We also test our results for H_0 in the following section using only the individual, rather than group, velocities. In all cases, we use velocities referenced to the CMB frame and downloaded through the Extragalactic Distance Database[7] (EDD; Tully et al. 2009). In fitting for H_0, we use the first-order cosmological corrections to the redshift (e.g., Wright 2006) assuming $\Omega_m = 0.3$, $\Lambda = 0.7$; the results change imperceptibly if we instead use the best-fit Planck values (0.315, 0.685) for a flat universe.

In the following section, we also calculate H_0 using the flow-corrected velocities predicted by two different models. The first is the Bayesian linear flow model of Graziani et al. (2019), based on the CosmicFlows-3 (CF3) database described by Tully et al. (2016). To implement this CF3 flow model for our sample, we use the online distance–velocity calculator[8] described by Kourkchi et al. (2020a). The model returns the distance expected from the observed velocity in the Local Group frame. To convert this model distance into the desired flow-corrected recessional velocity (i.e., Hubble expansion velocity), one must multiply it by the value of the Hubble constant most consistent with the CF3 database. The question of what value of H_0 to "take out" of the CF3 model in order to convert to expansion velocity is not entirely trivial. This value is a function of the zero point used for SNe Ia in the CF3 database and in that sense is independent of the H_0 we derive from our distances when using this velocity model. Tully et al. (2016) find $H_0 = 76.2$ km s^{-1} Mpc^{-1} to be the best-fit value for the CF3 database. In constructing the flow model, Graziani et al. (2019) assumed a fiducial $H_0 = 75$ km s^{-1} Mpc^{-1}, then, as part of the modeling, derived a best-fit scale factor of 1.02 ± 0.01, i.e., $H_0 = 76.5 \pm 0.8$ km s^{-1} Mpc^{-1}. To calculate the flow-corrected velocities for this model, we adopt the best-fit H_0 given by Tully and test the effect of the $\pm 1\%$ scale factor uncertainty on our result. When using this model, the scaling does affect our final H_0, as discussed below.

The second flow model is that of Carrick et al. (2015), based on the density field reconstructed from the 2M++ redshift compilation (Lavaux & Hudson 2011), which combines the 2MRS with deeper redshift surveys over large fractions of the sky. We again use the online velocity calculator[9] provided for the model. Unlike the CF3 model, the 2M++ model calculator requires the input velocity to be in the CMB frame.

4. The Hubble Constant

The 63 galaxies in our sample have SBF distances ranging from 19 to 99 Mpc, were selected in a variety of ways, and span a range of environments. Even homogeneously selected galaxies, such as those in the MASSIVE sample, may exhibit diverse features that can complicate the SBF analysis. In determining H_0, we use a weighted average in the logarithm to ensure a symmetric treatment of the errors in distance modulus and velocity; this is the equivalent of a single parameter fit minimizing χ^2 for the sample. To test the robustness of our results, we have performed the fits to H_0 using numerous different cuts and subsamples, as well as the four different approaches to the galaxy recessional velocities described in the preceding section. The sections below present an illustrative range of these fits before settling on a preferred value. All information needed to reproduce and extend these tests is provided in J21.

4.1. Group Velocities

As a first approach, we use the group-averaged velocities in the CMB frame as described above. In doing this, it is necessary to adopt some value for the random dispersion of the groups and isolated galaxies within the general velocity field. Estimates of this small-scale peculiar velocity "noise" σ_p range from 100 to 300 km s^{-1}, depending on the sample considered (Masters et al. 2006; Hoffman et al. 2015; Graziani et al. 2019). Here we assume $\sigma_p = 240$ km s^{-1}, which we add in quadrature with the generally small error in the group mean velocity (taken as zero for isolated galaxies). This results in a mean total velocity error of 250 km s^{-1}, typical of many peculiar velocity surveys involving early-type galaxies in groups (e.g., Zaroubi et al. 2001; Hudson et al. 2004). It corresponds to a 5.4% velocity error at the median distance of our sample.

Table 1 presents the results of many different trial fits of H_0, beginning with the full sample of 63 galaxies with group-averaged velocities. For this case, we find $H_0 = 73.53 \pm 0.66$ km s^{-1} Mpc^{-1}, but with a χ^2 per degree of freedom $\chi^2_\nu = 1.19$, which means that either σ_p or our distance errors are underestimated for at least a portion of the sample. Because morphological irregularities can cause problems for the SBF method, we experimented by keeping only galaxies with morphological type $T \leqslant -3$ in the HyperLEDA database (Makarov et al. 2014). This selects 45 galaxies classified as ellipticals or early-type S0s; the fitted H_0 is virtually identical, but with a significantly lower $\chi^2_\nu = 1.02$. This is an acceptable fit for 44 degrees of freedom, indicating that the errors are a reasonable description of the scatter for this sample. However, with our high-resolution HST data, we can do better than cataloged types derived from ground-based surveys. In reducing the data, one of us (J.B.J.) made consistent note of the presence of dust, spiral structure, bars, and shells. This was done prior to deriving the distances so that knowledge of discrepant results could not bias the classification. Eleven galaxies show evidence of spiral structure or dust. However, one of these is NGC 4993, which has deep high-resolution ACS g_{475} imaging that clearly reveals the localized dust features, allowing them to be excised to give a clean area for the SBF measurement. A distance for this galaxy was already published by Cantiello et al. (2018b), and we keep it in our resulting sample of 53 "clean" galaxies while rejecting the other ten. Line 3 of Table 1 shows that this sample gives $H_0 = 73.44 \pm 0.71$ with $\chi^2_\nu = 0.97$, again indicating a good fit (further cuts of galaxies with shells, bars, etc., do not yield additional improvement). We also show results from a fit using only clean galaxies that were selected as part of MASSIVE, a well-defined mass-selected sample. Again, the value of H_0 is

[7] http://edd.ifa.hawaii.edu/
[8] http://edd.ifa.hawaii.edu/CF3calculator/api.php
[9] https://cosmicflows.iap.fr

Table 1
Hubble Constants for Various Selections

Selected Sample[a]	v[b]	N_{gxy}	χ^2_ν	H_0
All galaxies	grp	63	1.19	73.53 ± 0.66
Ellipticals	grp	45	1.02	73.52 ± 0.74
All clean	grp	53	0.97	73.44 ± 0.71
MASSIVE, clean	grp	37	1.16	73.86 ± 0.82
$d > 60$, clean	grp	34	0.88	73.33 ± 0.82
$d < 70$, clean	grp	33	0.88	74.08 ± 0.96
$d < 80$, clean	grp	46	0.96	72.78 ± 0.77
SN Ia hosts, clean	grp	20	0.68	73.31 ± 1.26
All galaxies	ind	63	1.53	73.31 ± 0.67
All clean	ind	53	0.95	73.27 ± 0.73
MASSIVE, clean	ind	37	0.86	73.79 ± 0.85
$d < 80$, clean	ind	46	1.02	72.96 ± 0.76
All galaxies	cf3	63	1.14	73.32 ± 0.71
All clean	cf3	53	1.05	73.30 ± 0.76
MASSIVE, clean	cf3	37	1.16	73.62 ± 0.88
$d < 80$, clean	cf3	46	1.07	72.67 ± 0.83
All clean, -1%[c]	cf3	53	1.03	72.54 ± 0.76
All clean, $+1\%$[c]	cf3	53	1.06	74.07 ± 0.77
All galaxies	2M++	63	0.99	73.90 ± 0.65
All clean	2M++	53	0.89	73.78 ± 0.69
Massive, clean	2M++	37	1.02	74.09 ± 0.80
$d < 80$, clean	2M++	46	0.94	73.42 ± 0.75

Notes.
[a] "Ellipticals" refers to morphological type $T \leqslant -3$; "clean" indicates galaxies with no discernible dust or spiral structure; "MASSIVE" means limited to MASSIVE Survey galaxies.
[b] Velocities used for the fit: grp for group-averaged; ind for individual galaxy; cf3 for the flow model of Graziani et al. (2019); 2M++ for the flow model of Carrick et al. (2015).
[c] Velocities from the CF3 linear flow model rescaled by $\pm 1\%$

consistent, but χ^2_ν increases, likely because the adopted σ_p works well on average but slightly underestimates the small-scale dispersion of galaxy groups embedded within rich environments. A value of $\sigma_p = 275$ km s^{-1} would give $\chi^2_\nu = 1.0$ with a negligible change to H_0.

Figure 1 (left panel) presents the Hubble diagram combining our SBF distances with the group-averaged velocities, along with the best-fit H_0 value for the clean sample. The figure also shows the values of H_0 derived from individual galaxies. The scatter decreases at larger distance as the velocity errors become a smaller fraction of the recession velocity. Overall, the fit is good, but by eye, there is a suggestion of small-scale coherent trends, with several galaxies near ~75 Mpc lying below the line and three near ~90 Mpc scattering above. Features in the Hubble diagram can be associated with small-scale coherent flows. There is an ongoing HST/WFC3 SBF program exploring this issue in more detail.

Alternatively, if we were inadequately accounting for the effects of globular clusters in the power spectra of the most distant galaxies, this could cause those galaxies to scatter to high H_0. We have explored a number of cuts in distance for our clean sample; the table shows three examples: excluding galaxies within 60 Mpc, excluding those beyond 70 Mpc, or beyond 80 Mpc. In all these cases, $\chi^2_\nu < 1$. The nearer galaxies have little leverage on H_0, and removing them has little effect. Changing the upper distance limit can change H_0 by up to $\pm 1\%$, but this is still within the statistical error.

Finally, we also show the results from a fit using only clean galaxies that are identified as SN Ia hosts. These galaxies range in distance from 19 to 91 Mpc, with the few most distant ones having two orbits of integration. The best-fit H_0 is similar to that derived for the full clean sample, but the statistical uncertainty is much larger because the fit includes only 20 galaxies.

4.2. Individual Velocities

We performed a second set of fits using individual galaxy velocities from the 2MRS referenced to the CMB frame. However, we know that two-thirds of our sample consist of massive ellipticals that preferentially reside in rich groups and clusters that can have velocity dispersions up to 900 km s^{-1}. Thus, the assumption of a fixed random velocity error is insufficient. The Tully (2015) group catalog provides line-of-sight velocity dispersions for all groups, and these can be used as estimates of the random velocity errors for the member galaxies (neglecting the random motion of the groups themselves). We adopt this approach: using the individual galaxy velocities with the errors taken to be the dispersions of the parent groups. For galaxies not in groups, we adopt an error of 150 km s^{-1}, consistent with the quoted velocity field error in isolated regions from Graziani et al. (2019).

The second section of Table 1 shows example fits using this approach. Interestingly, the subsample of clean MASSIVE galaxies now gives the lowest χ^2_ν. This is likely because the most massive members of groups and clusters tend to deviate from the mean by less than one standard deviation, although there are exceptions in our sample such as NGC 1272 in Perseus, which has a velocity 1600 km s^{-1} below the cluster mean. Overall, the H_0 values from these fits track those from the group velocity fits to within ~0.2 km s^{-1} Mpc^{-1}.

4.3. Flow-corrected Model Velocities

The lines labeled "cf3" in the second column of Table 1 show results obtained using the flow-corrected recessional velocities from the CF3 linear velocity model of Graziani et al. (2019), implemented as described in Section 3. For the velocity error in this case, we use the model's best-fit nonlinear dispersion value of 280 km s^{-1}, which represents the unmodeled small-scale motion in the velocity field. The results of these tests are very similar to those found using the individual CMB-frame velocities. The χ^2_ν values are a bit higher in most cases, but there is no significant change in H_0.

We perform two other fits for this model, varying the scale factor of the velocity field within the reported $\pm 1\%$ uncertainty. Unsurprisingly, this changes the H_0 we derive by $\pm 1\%$ as well. Because the result given by the baseline scale factor agrees well with that found using the uncorrected CMB-frame velocities, this change in H_0 would represent a net inward or outward flow of our sample with respect to the comoving volume (a small Hubble bubble or sinkhole). Until we have more complete high-precision distance mapping of the local volume extending beyond 100 Mpc, we take this $\pm 1\%$ as the systematic uncertainty in the velocity scale.

Finally, the fits in Table 1 identified as "2M++" use the flow-corrected recessional velocities from the density-based model of Carrick et al. (2015), also described in Section 3. As for the group velocity fits above, we again use $\sigma_p = 240$ km s^{-1}. We find that the corrected velocities from this model result in

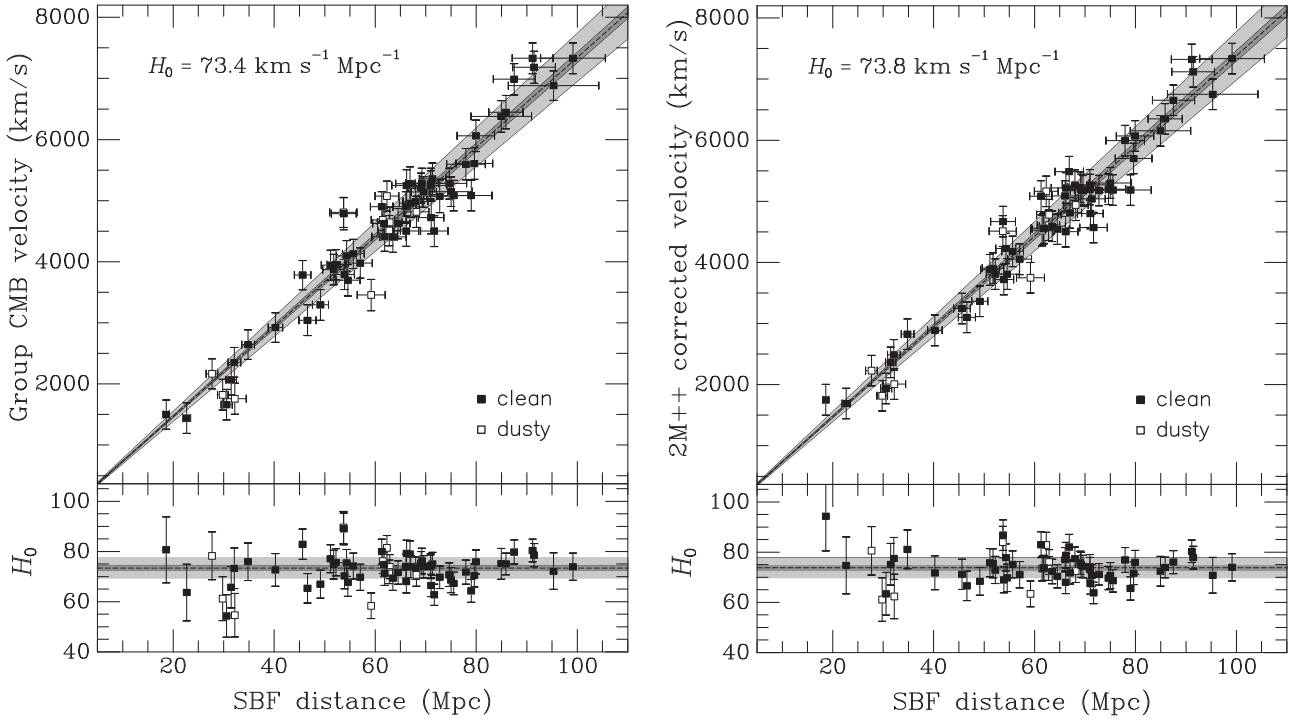

Figure 1. Left: Hubble diagram (top) and individual H_0 values (bottom) for the Cepheid-calibrated WFC3/IR SBF distances and the galaxy group-averaged velocities in the CMB rest frame. Solid symbols indicate "clean" galaxies, for which no dust or spiral structure is evident. The open symbols indicate galaxies with obvious dust and/or spiral structure. The represented Hubble constant is the best-fitting value for the "clean" galaxy sample using these distances and velocities; the statistical and systematic error ranges are shown in dark and light gray, respectively. The plotted H_0 error bars include both velocity and distance errors. Right: same as the plot on the left, except using the flow-corrected recessional velocities derived from the 2M++ density field analysis of Carrick et al. (2015). The scatter is reduced by these flow-corrected velocities. Note that the distances would uniformly increase, and H_0 decrease, by 0.3% for the TRGB-based SBF calibration (see Appendix).

significant improvements in χ^2_ν with respect to the other sets of velocities. For instance, the unreduced χ^2 for the full sample drops by $\Delta\chi^2 > 12$ compared to the fit using the group-averaged velocities. The resulting H_0 values are $\sim$0.4 km s^{-1} Mpc^{-1} higher, again consistent within the errors. The Hubble diagram in the right panel of Figure 1 illustrates the slightly higher value of H_0 and reduced scatter when using the 2M++ model velocities.

4.4. *Final* H_0

For the preferred H_0 from our analysis, we adopt the result in Table 1 for the full "clean" sample using the group velocities. Although the 2M++ model velocities gave lower values of χ^2_ν, we suspect that the model-independent group velocities may be more robust against systematic errors in scaling. We note that the same approach was used by Pesce et al. (2020) in deriving H_0 from their maser distances, for which the 2M++ model similarly gave the best fit. Readers who prefer the H_0 result based on the 2M++ model should increase the values given in this section by 0.5%. Thus, we adopt $H_0 = 73.44 \pm 0.71$ km s^{-1} Mpc^{-1}, statistical error only, for our Cepheid-calibrated value of H_0. The revised Cepheid-based SBF calibration has a systematic uncertainty of 0.09 mag, or 4.2% in distance (Section 2.4), translating to $\pm$3.11 km s^{-1} Mpc^{-1} for H_0.

In the Appendix, we find that the TRGB-based calibration differs by 0.007 ± 0.099 mag from the Cepheid calibration, in the sense that the SBF distances increase by $\sim$0.3%. The TRGB calibration therefore gives $H_0 = 73.20$ km s^{-1} Mpc^{-1}, with a systematic uncertainty of 4.7%, or $\pm$3.41 km s^{-1} Mpc^{-1}. Averaging these two independent calibrations gives 73.33 km s^{-1} Mpc^{-1} with a systematic error in the distance scale of 3.1%. We combine this in quadrature with the estimated 1% systematic error in the velocity scaling (Section 4.3) to give a total systematic error of 3.3%, or 2.41 km s^{-1} Mpc^{-1}. Our final result, to single decimal-point precision, is then $H_0 = 73.3 \pm 0.7 \pm 2.4$ km s^{-1} Mpc^{-1}. This calculation is summarized in Table 2.

Table 2
Final Hubble Constant and Errors

SBF Calibration	H_0[a]	σ_{stat}[b]	$\sigma_{sys}(d)$[c]	$\sigma_{sys}(v)$[d]
Cepheid	73.44	1.0%	4.1%	1.0%
TRGB	73.20	1.0%	4.7%	1.0%
Average	73.33	1.0%	3.1%	1.0%

Final: $H_0 = 73.3 \pm 0.7 \pm 2.4$ km s^{-1} Mpc^{-1}

Notes.
[a] H_0 for "clean" galaxy sample with group velocities.
[b] Statistical error from the H_0 fit.
[c] Systematic uncertainty in distance calibration.
[d] Systematic uncertainty in velocity scaling.

5. Context

Verde et al. (2019) referenced a preliminary value of H_0 from this project presented at a 2019 Kavli workshop (Blakeslee 2019). The value presented here is 4% lower than the preliminary one. There have been several changes in our analysis since that workshop. First, we have added nine more galaxies to our WFC3/IR sample, improving our constraints. Second, as discussed by J21, we have improved our masking

technique for removing background sources. This has a negligible effect for most galaxies in our sample, but becomes marginally significant for the most distant galaxies with only one orbit of integration; we explored this issue in our tests above by imposing distance cutoffs on the sample.

However, the main reason for the decrease in H_0 was our switch from the velocities given by the Mould et al. (2000) parametric attractor model to those used here. As noted by Tonry et al. (2000), models that add massive attractors without compensating to ensure zero net change to Ω_m can bias H_0 high if the galaxies preferentially lie beyond the attractors, as is the case here for the Virgo and Great Attractor components of the Mould model. We note that Pesce et al. (2020) saw the same effect: their H_0 increased by 4% when they used the Mould model velocities. Given the consistency of our results for four different treatments of the recessional velocities, including two recent flow models, we are confident that the H_0 presented here is far more robust than the earlier one.

As discussed in the Introduction, many of the previous measurements of H_0 using the SBF method relied on other techniques to tie local SBF distances to the far-field Hubble flow. A recent example is by Khetan et al. (2020), who used a heterogeneous set of 24 ground-based and HST SBF distances to calibrate the SN Ia peak luminosity and then derived H_0 from 96 SNe Ia at larger distances. That study used essentially the same distance calibration as us, except for the adjustment we made for the improved LMC distance. Including this revision, the Khetan et al. (2020) value becomes $H_0 = 71.1 \pm 2.4 \pm 3.4$ km s^{-1} Mpc^{-1} (statistical and systematic errors), which agrees with our result to within the statistical error. Of course, because there are significantly fewer Cepheid calibrators for the SBF method than for SNe Ia, using SBF as an intermediary will result in a lower precision of H_0. Nonetheless, SBF distances remain an extremely promising way of exploring possible systematics in SN Ia properties; HST program GO-14654 was predicated on this very goal and has provided nearly a third of our WFC3/IR SBF sample. Our results from this program will be presented in future works (P. Garnavich et al. 2021, in preparation; P. Milne et al. 2021, in preparation).

Although ours is the first measurement of H_0 from a statistical sample of WFC3/IR SBF distances, Jensen et al. (2001) previously derived $H_0 = 76 \pm 1.3 \pm 6$ km s^{-1} Mpc^{-1} from IR SBF distances for 16 galaxies, ranging from 40 to 130 Mpc observed with NICMOS. When considering only the six most distant galaxies, their value was $72 \pm 2.3 \pm 6$ km s^{-1} Mpc^{-1}. However, as discussed in that work, the NICMOS images suffered persistent residuals from cosmic rays that affected the image power spectra to an uncertain degree. Further, the NICMOS SBF calibration, explored in more detail by Jensen et al. (2003), was not well constrained for stellar population effects, and Blakeslee et al. (2010) discuss a possible systematic shift in the NICMOS distance moduli. In contrast, the WFC3/IR SBF calibration by Jensen et al. (2015), with the small revisions discussed in Section 2.4 above, provides a firm foundation for the current H_0 measurement.

Another direct SBF H_0 measurement was by Biscardi et al. (2008) who analyzed ACS/F814W images of four galaxies with distances of 55–110 Mpc. Interestingly, these authors opted for a theoretical calibration from the stellar population models of Raimondo (2009). Their result was $H_0 = 76 \pm 6 \pm 5$ km s^{-1} Mpc^{-1}, where the second error bar reflects their estimated uncertainty in the model calibration. Further refinements to the models, perhaps incorporating constraints from Gaia, could make this a competitive calibration route for SBF.

Cantiello et al. (2018b) previously demonstrated the usefulness of single-orbit WFC3/IR observations for precise SBF distances out to at least 40 Mpc and reported a Hubble constant $H_0 = 71.9 \pm 7.1$ km s^{-1} Mpc^{-1} (or 72.5 ± 7.2 with the revision to the LMC distance). Because that sample consisted of only NGC 4993, the host galaxy of the GW 170817 event, the total error was dominated by statistical effects, including both the distance measurement error and the random error in the peculiar velocity. With the present sample of over 60 galaxies, NGC 4993 among them, the statistical error in H_0 has dropped below the 1% level.

In the broader context, our result is consistent with recent values of H_0 from Cepheid-calibrated SN Ia and Tully–Fisher distances in the local universe, as well as Cepheid-independent results from water masers and gravitationally lensed image delay times (see references in the Introduction). It disagrees with the predicted value from Planck for the ΛCDM cosmology at the 2.3σ level. Although our measurement is by far the most direct and precise value of H_0 from SBF to date, it could be improved substantially through a better constraint on the distance zero point. We conclude by suggesting one possibility for accomplishing this goal.

6. Summary and Outlook

We have presented a new measurement of the Hubble constant based on a homogeneous set of 63 WFC3/IR SBF distances extending out to 100 Mpc. The data are provided in a companion paper (J21). Two-thirds of our sample are luminous early-type galaxies selected as part of the MASSIVE Survey; most of the rest were selected as hosts of recent SNe Ia. We have performed numerous tests, including four different treatments of the galaxy velocities, to ensure that our result is robust within the quoted errors. Although the 2M++ flow model gives the lowest scatter in the Hubble diagram, we use the observed group-averaged velocities to retain model independence. Averaging the results for the Cepheid and TRGB calibrations of SBF, our final result is $H_0 = 73.3 \pm 0.7 \pm 2.4$ km s^{-1} Mpc^{-1}, where the error bars represent the statistical and systematic uncertainties. This agrees well with other recent measurements of H_0 in the local universe.

Of the 63 galaxies in our WFC3/IR SBF data sample, 24 have hosted SNe Ia with high-quality light-curve data. The intercomparison of these two precision distance indicators enables a detailed investigation of subtle effects in both methods (P. Milne et al. 2021, in preparation). It may also provide a better absolute calibration of the SBF zero point because SNe Ia have been tied to Cepheids through a larger number of calibrating galaxies. Additionally, we have an ongoing WFC3/IR SNAP program that will further improve our constraints on H_0 and the velocity structure of the local universe. At the same time, more extensive stellar population modeling in the near-infrared, implementing new constraints on the luminosities and lifetimes of evolved stars in metal-rich populations (e.g., Villaume et al. 2017; Pastorelli et al. 2020), can help us understand better the deviations of some galaxies

from the IR SBF versus color relation, perhaps leading to an improved distance method.

Although WFC3/IR has proven to be a powerful tool for SBF measurements, reaching 80 to 100 Mpc with 4%–5% distance precision in a single HST orbit, the systematic uncertainty in the SBF zero point currently limits the method's ability to achieve competitive constraints on cosmology. However, prospects have never been better for improvement. In addition to a tighter tie with Cepheids through the SN Ia comparison mentioned above, SBF is ideally suited for calibration via the TRGB method. We document our initial SBF–TRGB calibration in the Appendix of this work, which shows excellent agreement between SBF and TRGB distances for two giant ellipticals in Virgo. The impending launch of the James Webb Space Telescope (JWST) will enable numerous more TRGB distances to Virgo ellipticals in only modest amounts of observing time.

The systematic uncertainty in the TRGB absolute magnitude is approaching 2% (see Appendix). If it can be reduced further through a combination of different approaches to the same 1.3% level as for Cepheids, that would open the door to a 2% constraint on the SBF zero point from a sample of 15 galaxies having both high-quality TRGB and SBF distances. This estimate assumes realistic errors for both methods. A single medium-sized JWST proposal could achieve this goal and give rise to a fully independent TRGB–SBF precision ladder, competitive with the Cepheid–SN Ia ladder, for testing the significance of the discrepancy between local and CMB-based measurements of H_0. We look forward to ascending that ladder.

We are grateful to Gabe Brammer for assistance with processing the raw WFC3/IR data; Brent Tully for guidance with the CF3 velocity data; and Adam Riess, Dan Scolnic, and John Tonry for helpful conversations. Support for this work was provided by NASA through grants HST-GO-14219, HST-GO-14654, and HST-GO-15265 from the Space Telescope Science Institute, which is operated by AURA, Inc., under NASA contract NAS 5-26555. The MASSIVE Survey is supported in part by NSF grants AST-1815417 and AST-1817100. C.-P.M. acknowledges support from the Heising-Simons Foundation and the Miller Institute for Basic Research in Science. This work was also supported by the International Gemini Observatory, a program of NSFs NOIRLab, which is managed by the Association of Universities for Research in Astronomy under a cooperative agreement with the National Science Foundation, on behalf of the Gemini partnership of Argentina, Brazil, Canada, Chile, the Republic of Korea, and the United States of America. This paper is dedicated to the memory of Justin Ross Dougherty, a dear friend we lost while this was being written; he so loved the concept of appendices.

Facilities: HST (WFC3/IR, ACS), Pan-STARRS.

Appendix
SBF Zero Point from the Tip of the Red Giant Branch

The SBF method works best with evolved stellar populations in morphologically regular early-type galaxies. Cepheids do not exist in such galaxies, but the TRGB method is well suited for measuring their distances, and there have been initial efforts to calibrate the TRGB with Gaia (Soltis et al. 2021). This is an extremely promising route for calibrating SBF via a direct tie to a geometrically calibrated distance indicator. Here we take a first step along this route.

A.1. Absolute Magnitude of the TRGB

Before tying SBF to the TRGB method, we must enforce that the galaxies all use the same TRGB absolute magnitude calibration. Numerous TRGB calibrations have been published recently; we list them for reference in Table 3. Some of the calibrations are quoted in the HST F814W bandpass, $M_{814}^{\rm TRGB}$, while others are in the standard Cousins I band, $M_I^{\rm TRGB}$. To convert between the two, we use the following transformation from Riess et al. (2016) with the TRGB color assumed by Freedman et al. (2019):

$$M_{814}^{\rm TRGB} = M_I^{\rm TRGB} + 0.02 - 0.018(V-I); \quad \text{(A1)}$$

$$M_{814}^{\rm TRGB} \approx M_I^{\rm TRGB} - 0.009. \quad \text{(A2)}$$

Thus, $M_I^{\rm TRGB} \approx M_{814}^{\rm TRGB} + 0.01$. For ease of comparison, the fourth column of Table 3 shows the value of $M_I^{\rm TRGB}$, rounded to the nearest hundredth, for each of the recent TRGB calibrations. Several of these take their zero point from the LMC, using the DEB distance of Pietrzyński et al. (2019), as we did in adjusting the Cepheid zero point for SBF. In order to keep the two SBF calibrations independent, we prefer to use a TRGB calibration based on another geometric method, the maser distance to NGC 4258. For this purpose, we take a simple average of the recent results of Reid et al. (2019) and Jang et al. (2020) using this approach. Because these studies use the same basic distance and photometric data, averaging them does not reduce the error, and we adopt

$$M_I^{\rm TRGB} = -4.02 \pm 0.05 \text{mag}. \quad \text{(A3)}$$

This is very close to the value derived by Jang & Lee (2017) and the reassessment by Capozzi & Raffelt (2020) combining the distance from Reid et al. (2019) with the photometric measurements of Jang & Lee (2017).

Ultimately, the best calibration of $M_I^{\rm TRGB}$ will come from Gaia, and the recent result of Soltis et al. (2021) in Table 3, using Gaia Early Data Release 3 (EDR3) parallaxes, is promising. Thus far, however, it is based on only the single large globular cluster ω Cen, likely the remnant nucleus of a stripped dE (e.g., Hilker & Richtler 2000; Majewski et al. 2000). Capozzi & Raffelt (2020) use the same ω Cen photometric data but adopted the kinematic distance from Baumgardt et al. (2019) based on Gaia EDR2 data. Cerny et al. (2020) use Gaia EDR2 proper motion data to assign membership for a sample of 46 globular clusters and determine their relative distances from the horizontal branch; the zero point is set from the DEB distance to ω Cen. We look forward to the analysis of the TRGB in an expanded sample of globular clusters using Gaia parallaxes. This will also enable a determination of the intrinsic scatter in the TRGB absolute magnitude, an error term that is generally ignored.

A.2. Tying the SBF Method to the TRGB

Blakeslee et al. (2009) tabulate high-quality HST/ACS SBF distances for 134 early-type galaxies mainly in the Virgo and Fornax clusters, and Jensen et al. (2015) present similar quality WFC3/IR SBF measurements for 16 of these galaxies. These

Table 3
Ten Recent TRGB Absolute Calibrations

Reference (1)	Band (2)	$M_{\rm Band}^{\rm TRGB}$ (mag) (3)	$M_I^{\rm TRGB}$ (mag) (4)	$\sigma_{\rm tot}$ (mag) (5)	$\sigma_{\rm stat}$ (mag) (6)	$\sigma_{\rm sys}$ (mag) (7)	Anchoring Method (8)
Freedman et al. (2019)	F814W	−4.049	−4.04	0.045	0.022	0.039	DEB distance to LMC[a]
Yuan et al. (2019)	F814W	−3.970	−3.96	0.046	0.038	0.026	DEB distance to LMC[b]
Freedman et al. (2020)	*I*	−4.047	−4.05	0.045	0.022	0.039	DEB distance to LMC[a]
Soltis et al. (2021)	*I*	−3.961	−3.96	0.040	0.011	0.038	DEB distance to LMC[c]
Reid et al. (2019)	F814W	−4.012	−4.00	0.044	0.030	0.032	Maser distance to NGC 4258
Jang et al. (2020)	F814W	−4.050	−4.04	0.056	0.028	0.048	Maser distance to NGC 4258
Capozzi & Raffelt (2020)	*I*	−4.027	−4.03	0.055	0.045	0.032	Maser distance to NGC 4258
Capozzi & Raffelt (2020)	*I*	−3.960	−3.96	0.067	0.064	0.021	GAIA EDR2 kinematic d to ω Cen
Soltis et al. (2021)	*I*	−3.970	−3.97	0.062	0.041	0.047	GAIA EDR3 parallax d to ω Cen
Cerny et al. (2020)	*I*	−4.056	−4.06	0.10	0.022	0.101	HB for 46 GCs + DEB in ω Cen[d]

Notes. Columns list: (1) calibration paper; (2) reference band used in the study (Vega-based calibrations); (3) derived TRGB absolute magnitude in reference band; (4) absolute TRGB magnitude in standard Cousins *I*, assuming where needed $I = m_{814W} + 0.009$, and rounded to the nearest hundredth; (5) total error quoted from the study, or quadrature sum of quoted random and systematic errors; (6) quoted statistical error or derived from information provided; (7) quoted systematic error or derived from information provided; (8) distance method used for anchoring the zero point.
[a] Extinction determined from observed TRGB color differences.
[b] Extinction from the Haschke et al. (2011) OGLE reddening map.
[c] Extinction from the Skowron et al. (2021) OGLE reddening map.
[d] "HB" refers to the horizontal branch, used by Cerny et al. (2020) to shift the 46 globular clusters (GCs) into agreement before setting the distance zero point based on a DEB in ω Cen (Thompson et al. 2001).

Table 4
Homogenized SBF–TRGB Distance Comparisons

Galaxy	$(m-M)_{\rm SBF}$[a] (mag)	$\sigma_{\rm SBF}$ (mag)	$(m-M)_{\rm TRGB}$[b] (mag)	$\sigma_{\rm TRGB}$ (mag)	$\Delta(m-M)$[c] (mag)	σ_Δ[c] (mag)	Reference for TRGB
NGC 4486/M87	31.088	0.079	31.09	0.10	−0.002	0.128	Bird et al. (2010)
NGC 4649/M60	31.059	0.076	31.07	0.07	−0.011	0.103	Lee & Jang (2017)
NGC 1316	31.583	0.073	31.44	0.04	+0.143	0.083	Hatt et al. (2018); Freedman et al. (2019)
weighted average for Virgo galaxies: $\langle\Delta(m-M)\rangle = -0.007 \pm 0.080$							
weighted average for all three galaxies: $\langle\Delta(m-M)\rangle = +0.065 \pm 0.058$							

Notes.
[a] SBF distance moduli from Blakeslee et al. (2009), reduced by 0.023 mag as described in Section 2.4; $\sigma_{\rm SBF}$ is the statistical error as published.
[b] TRGB distance moduli from references in the last column, corrected by −0.03, +0.02, and −0.02 mag (M87, M60, and NGC 1316, respectively) for consistency with our adopted zero point of $M_I^{\rm TRGB} = -4.02$ mag ($M_{814}^{\rm TRGB} = -4.03$ mag), which is an average of two recent TRGB calibrations based on the NGC 4258 maser distance (Reid et al. 2019; Jang et al. 2020). The statistical errors $\sigma_{\rm TRGB}$ are as published; unlike the SBF errors, they include no allowance for intrinsic scatter in the absolute magnitude of the standardized candle.
[c] Difference in distance moduli: $(m-M)_{\rm SBF} - (m-M)_{\rm TRGB}$, and error in this difference σ_Δ.

samples enabled the calibration of the color dependence of the SBF magnitude in the giant ellipticals that we measure at large distances. We wish to tie these calibration samples to the TRGB method in order to improve the SBF zero-point calibration.

Unfortunately, there are few TRGB distances to giant ellipticals. Two exceptions are M60/NGC 4649 (Lee & Jang 2017) and M87/NGC 4486 (Bird et al. 2010). While not ideal, the giant, dusty merger remnant NGC 1316 (Arp 154, Fornax A) is another galaxy that has a high-quality HST-based SBF distance and a published TRGB distance (Hatt et al. 2018). Table 4 displays the SBF and TRGB distances for the three galaxies. The SBF distances in this table are the homogeneous set from Blakeslee et al. (2009), adjusted to the revised LMC distance based on DEBs (see Section 2.4). The TRGB distances have been adjusted for consistency with our adopted calibration in Equation (A3). For NGC 1316, we use the revised TRGB distance given by Freedman et al. (2019) before adjusting to our adopted calibration.

We note that Freedman et al. (2019), with the goal of increasing the number of TRGB–SN Ia calibrators, also tabulate a "TRGB distance," with a purported precision of 0.05 mag, for NGC 1404, a giant elliptical just 50 kpc from the cD NGC 1399 in the core of the Fornax cluster. We have excellent SBF distances for these two galaxies. However, the quoted TRGB distance is actually an average of the TRGB distances to the spiral galaxy NGC 1365 and the merger remnant NGC 1316. NGC 1365 lies 420 kpc in projection from the Fornax core, has an angular size larger than any of the Fornax ellipticals and has been suggested to lie significantly in the foreground (Saha et al. 1997). NGC 1316 is projected 1.25 Mpc from the core; if the separation along the line of sight is the same, the offset would be 0.14 mag. There is no evidence

that these two late-type galaxies at substantial separations from the core have distance moduli within 0.05 mag of NGC 1404. Thus, we cannot use it as a TRGB calibrator.

Table 4 reports the weighted average offsets between the SBF and TRGB distances when using just M60 and M87 in Virgo, and when using NGC 1316 as well. These averages differ by 0.07 mag. While this is in statistical agreement, given that we have so few calibrators, we want to ensure that all individual measurements are reliable. NGC 1316 is an irregular galaxy with prominent dust features, Hα filaments, tidal loops, and shells indicative of recent merging (Schweizer 1980). Based on the ages of the centrally concentrated population of bright, metal-rich star clusters, the galaxy is believed to have undergone a major merger, with an associated starburst, 2–3 Gyr ago (Goudfrooij et al. 2001; Sesto et al. 2018). The IR SBF magnitude for NGC 1316 is 0.25 mag brighter than expected based on the color calibration defined by more evolved early-type galaxies. This is consistent with predictions from stellar population models if there is a 3 Gyr old population present (Jensen et al. 2015). In contrast, optical SBF distances are less affected by younger populations because their effect is to move the galaxy both brighter and bluer along the SBF–color relation, rather than simply scattering the SBF magnitude brighter. For this reason, we have more confidence in the optical SBF distance (shown in Table 4) for this galaxy than the IR one.

At present, the star formation in NGC 1316 is mainly occurring at larger radius. Based on the mid-IR emission, Temi et al. (2005) suggest that "young, luminous stars are forming in the infalling dusty gas, raising the dust temperature sufficiently to emit at 15 μm." Thus, unlike in spiral galaxies, where the star formation occurs in an orderly fashion in the disk while the halo hosts only ancient metal-poor stars, NGC 1316 appears to have a significant population of young stars at large radius. Notably, the field used for the TRGB measurement was about 10′ from the galaxy's center, in an area of intense radio emission (Ekers et al. 1983). We suspect that a dispersed population of asymptotic giant branch stars associated with the prominent 3 Gyr, and perhaps younger, component may have biased the TRGB measurement. More dramatic biases have occurred in TRGB estimates for more recent mergers at roughly the same distance (Schweizer et al. 2008). The young component at large radius in NGC 1316 could account for the observed difference in the TRGB and optical SBF distances for this galaxy.

In short, we lack confidence in NGC 1316 as a reliable calibrator. We therefore adopt the mean offset of -0.007 ± 0.080 mag between the TRGB and SBF distances, determined from the two giant ellipticals in Virgo. Including the 0.03 mag error in the tie between the optical and IR SBF distances and the 0.05 mag error in the TRGB calibration, the final offset and uncertainty in the SBF zero point from this TRGB comparison is -0.007 ± 0.099 mag, which we round to -0.01 ± 0.10 mag in Section 2.5 of the present work.

Ideally, we would make a direct tie between geometrically calibrated TRGB distances to giant ellipticals and the IR SBF measurements to the same galaxies, avoiding the 0.03 mag error incurred from the tie through the more extensive optical SBF data set. However, at present, M60 is the only IR SBF calibrator from Jensen et al. (2015) with a TRGB distance. The result would be similar, but with a larger error. Section 6 presents a plan for improving this situation.

ORCID iDs

John P. Blakeslee https://orcid.org/0000-0002-5213-3548
Joseph B. Jensen https://orcid.org/0000-0001-8762-8906
Chung-Pei Ma https://orcid.org/0000-0002-4430-102X
Peter A. Milne https://orcid.org/0000-0002-0370-157X
Jenny E. Greene https://orcid.org/0000-0002-5612-3427

References

Addison, G. E., Watts, D. J., Bennett, C. L., et al. 2018, ApJ, 853, 119
Bailer-Jones, C. A. L., Rybizki, J., Fouesneau, M., Mantelet, G., & Andrae, R. 2018, AJ, 156, 58
Bajaj, V., Calamida, A., & Mack, J. 2020, Updated WFC3/IR Photometric Calibration, Space Telescope WFC Instrument Science Report, Space Telescope Science Institute
Baumgardt, H., Hilker, M., Sollima, A., & Bellini, A. 2019, MNRAS, 482, 5138
Bird, S., Harris, W. E., Blakeslee, J. P., & Flynn, C. 2010, A&A, 524, A71
Biscardi, I., Raimondo, G., Cantiello, M., & Brocato, E. 2008, ApJ, 678, 168
Blakeslee, J. P. 2012, Ap&SS, 341, 179
Blakeslee, J. P. 2019, in KITP Conference: Tensions between the Early and the Late Universe (Santa Barbara, CA: Univ. California), 18
Blakeslee, J. P., Ajhar, E. A., & Tonry, J. L. 1999a, Distances from Surface Brightness Fluctuations, 237 (Dordrecht: Kluwer Academic), 181
Blakeslee, J. P., & Cantiello, M. 2018, RNAAS, 2, 146
Blakeslee, J. P., Cantiello, M., Mei, S., et al. 2010, ApJ, 724, 657
Blakeslee, J. P., Davis, M., Tonry, J. L., Dressler, A., & Ajhar, E. A. 1999b, ApJL, 527, L73
Blakeslee, J. P., Jordán, A., Mei, S., et al. 2009, ApJ, 694, 556
Blakeslee, J. P., Lucey, J. R., Tonry, J. L., et al. 2002, MNRAS, 330, 443
Blakeslee, J. P., Vazdekis, A., & Ajhar, E. A. 2001, MNRAS, 320, 193
Brown, P. J., Hosseinzadeh, G., Jha, S. W., et al. 2019, ApJ, 877, 152
Brown, P. J., Landez, N. J., Milne, P. A., & Stritzinger, M. D. 2017, ApJ, 836, 232
Cantiello, M., Blakeslee, J., Raimondo, G., Brocato, E., & Capaccioli, M. 2007, ApJ, 668, 130
Cantiello, M., Blakeslee, J. P., Ferrarese, L., et al. 2018a, ApJ, 856, 126
Cantiello, M., Blakeslee, J. P., Raimondo, G., et al. 2005, ApJ, 634, 239
Cantiello, M., Grado, A., Blakeslee, J. P., et al. 2013, A&A, 552, A106
Cantiello, M., Jensen, J. B., Blakeslee, J. P., et al. 2018b, ApJL, 854, L31
Capozzi, F., & Raffelt, G. 2020, PhRvD, 102, 083007
Carlsten, S. G., Beaton, R. L., Greco, J. P., & Greene, J. E. 2019, ApJ, 879, 13
Carrick, J., Turnbull, S. J., Lavaux, G., & Hudson, M. J. 2015, MNRAS, 450, 317
Cerny, W., Freedman, W. L., Madore, B. F., et al. 2020, arXiv:2012.09701
Cohen, Y., van Dokkum, P., Danieli, S., et al. 2018, ApJ, 868, 96
Cook, J., & Mohr, J. M. 1771, RSPT, 61, 433
Crook, A. C., Huchra, J. P., Martimbeau, N., et al. 2007, ApJ, 655, 790
Di Valentino, E. 2021, MNRAS, 502, 2065
Di Valentino, E., Melchiorri, A., & Silk, J. 2020, NatAs, 4, 196
Ekers, R. D., Goss, W. M., Wellington, K. J., et al. 1983, A&A, 127, 361
Ene, I., Ma, C.-P., Walsh, J. L., et al. 2020, ApJ, 891, 65
Event Horizon Telescope Collaboration, Akiyama, K., Alberdi, A., et al. 2019, ApJL, 875, L6
Foley, R. J., Hoffmann, S. L., Macri, L. M., et al. 2020, MNRAS, 491, 5991
Freedman, W. L., Madore, B. F., Gibson, B. K., et al. 2001, ApJ, 553, 47
Freedman, W. L., Madore, B. F., Hatt, D., et al. 2019, ApJ, 882, 34
Freedman, W. L., Madore, B. F., Hoyt, T., et al. 2020, ApJ, 891, 57
Goudfrooij, P., Mack, J., Kissler-Patig, M., Meylan, G., & Minniti, D. 2001, MNRAS, 322, 643
Goullaud, C. F., Jensen, J. B., Blakeslee, J. P., et al. 2018, ApJ, 856, 11
Graziani, R., Courtois, H. M., Lavaux, G., et al. 2019, MNRAS, 488, 5438
Greco, J. P., van Dokkum, P., Danieli, S., Carlsten, S. G., & Conroy, C. 2021, ApJ, 908, 24
Greene, J. E., Janish, R., Ma, C.-P., et al. 2015, ApJ, 807, 11
Harvey, D. 2020, MNRAS, 498, 2871
Haschke, R., Grebel, E. K., & Duffau, S. 2011, AJ, 141, 158
Hatt, D., Freedman, W. L., Madore, B. F., et al. 2018, ApJ, 866, 145
Hilker, M., & Richtler, T. 2000, A&A, 362, 895, arXiv:astro-ph/0008500
Hoffman, Y., Courtois, H. M., & Tully, R. B. 2015, MNRAS, 449, 4494
Huchra, J. P., Macri, L. M., Masters, K. L., et al. 2012, ApJS, 199, 26
Hudson, M. J., Smith, R. J., Lucey, J. R., & Branchini, E. 2004, MNRAS, 352, 61
Jang, I. S., Hoyt, T., Beaton, R., et al. 2020, arXiv:2008.04181

Jang, I. S., & Lee, M. G. 2017, ApJ, 835, 28
Jensen, J. B., Blakeslee, J. P., Gibson, Z., et al. 2015, ApJ, 808, 91
Jensen, J. B., Blakeslee, J. P., Ma, C., et al. 2021, ApJ, in press
Jensen, J. B., Tonry, J. L., Barris, B. J., et al. 2003, ApJ, 583, 712
Jensen, J. B., Tonry, J. L., & Luppino, G. A. 1998, ApJ, 505, 111
Jensen, J. B., Tonry, J. L., Thompson, R. I., et al. 2001, ApJ, 550, 503
Khetan, N., Izzo, L., Branchesi, M., et al. 2020, arXiv:2008.07754
Knox, L., & Millea, M. 2020, PhRvD, 101, 043533
Kormendy, J., & Ho, L. C. 2013, ARA&A, 51, 511
Kourkchi, E., Courtois, H. M., Graziani, R., et al. 2020a, AJ, 159, 67
Kourkchi, E., Tully, R. B., Eftekharzadeh, S., et al. 2020b, ApJ, 902, 145
Lavaux, G., & Hudson, M. J. 2011, MNRAS, 416, 2840
Lee, M. G., & Jang, I. S. 2017, ApJ, 841, 23
Liepold, C. M., Quenneville, M. E., Ma, C.-P., et al. 2020, ApJ, 891, 4
Lindegren, L., Lammers, U., Bastian, U., et al. 2016, A&A, 595, A4
Ma, C.-P., Greene, J. E., McConnell, N., et al. 2014, ApJ, 795, 158
Macaulay, E., Nichol, R. C., Bacon, D., et al. 2019, MNRAS, 486, 2184
Macri, L. M., Ngeow, C.-C., Kanbur, S. M., Mahzooni, S., & Smitka, M. T. 2015, AJ, 149, 117
Magnier, E. A., Schlafly, E. F., Finkbeiner, D. P., et al. 2020, ApJS, 251, 6
Majewski, S. R., Patterson, R. J., Dinescu, D. I., et al. 2000, Liege International Astrophysical Coll. 35, Liege International Astrophysical Colloquia, ed. A. Noels et al., 619, arXiv:astro-ph/9910278
Makarov, D., Prugniel, P., Terekhova, N., Courtois, H., & Vauglin, I. 2014, A&A, 570, A13
Masters, K. L., Springob, C. M., Haynes, M. P., & Giovanelli, R. 2006, ApJ, 653, 861
McConnell, N. J., & Ma, C.-P. 2013, ApJ, 764, 184
Mei, S., Blakeslee, J. P., Côté, P., et al. 2007, ApJ, 655, 144
Mei, S., Blakeslee, J. P., Tonry, J. L., et al. 2005, ApJS, 156, 113
Milne, P. A., Brown, P. J., Roming, P. W. A., Bufano, F., & Gehrels, N. 2013, ApJ, 779, 23
Milne, P. A., Foley, R. J., Brown, P. J., & Narayan, G. 2015, ApJ, 803, 20
Mould, J. R., Huchra, J. P., Freedman, W. L., et al. 2000, ApJ, 529, 786
Nguyen, D. D., den Brok, M., Seth, A. C., et al. 2020, ApJ, 892, 68
Pastorelli, G., Marigo, P., Girardi, L., et al. 2020, MNRAS, 498, 3283
Pesce, D. W., Braatz, J. A., Reid, M. J., et al. 2020, ApJL, 891, L1
Philcox, O. H. E., Ivanov, M. M., Simonović, M., & Zaldarriaga, M. 2020, JCAP, 2020, 032
Pietrzyński, G., Graczyk, D., Gallenne, A., et al. 2019, Natur, 567, 200
Planck Collaboration, Aghanim, N., Akrami, Y., et al. 2020, A&A, 641, A6
Poulin, V., Smith, T. L., Karwal, T., & Kamionkowski, M. 2019, PhRvL, 122, 221301
Raimondo, G. 2009, ApJ, 700, 1247
Reid, M. J., Pesce, D. W., & Riess, A. G. 2019, ApJL, 886, L27
Riess, A. G., Casertano, S., Yuan, W., Macri, L. M., & Scolnic, D. 2019, ApJ, 876, 85
Riess, A. G., Macri, L. M., Hoffmann, S. L., et al. 2016, ApJ, 826, 56
Riess, A. G., Yuan, W., Casertano, S., Macri, L. M., & Scolnic, D. 2020, ApJL, 896, L43
Saha, A., Sandage, A., Labhardt, L., et al. 1997, ApJ, 486, 1
Sawyer Hogg, H. 1947, JRASC, 41, 319
Schlafly, E. F., & Finkbeiner, D. P. 2011, ApJ, 737, 103
Schweizer, F. 1980, ApJ, 237, 303
Schweizer, F., Burns, C. R., Madore, B. F., et al. 2008, AJ, 136, 1482
Sesto, L. A., Faifer, F. R., Smith Castelli, A. V., Forte, J. C., & Escudero, C. G. 2018, MNRAS, 479, 478
Skowron, D. M., Skowron, J., Udalski, A., et al. 2021, ApJS, 252, 23
Soltis, J., Casertano, S., & Riess, A. G. 2021, ApJL, 908, L5
Temi, P., Mathews, W. G., & Brighenti, F. 2005, ApJ, 622, 235
Thompson, I. B., Kaluzny, J., Pych, W., et al. 2001, AJ, 121, 3089
Tonry, J., & Schneider, D. P. 1988, AJ, 96, 807
Tonry, J. L., Ajhar, E. A., & Luppino, G. A. 1990, AJ, 100, 1416
Tonry, J. L., Blakeslee, J. P., Ajhar, E. A., & Dressler, A. 1997, ApJ, 475, 399
Tonry, J. L., Blakeslee, J. P., Ajhar, E. A., & Dressler, A. 2000, ApJ, 530, 625
Trujillo, I., Beasley, M. A., Borlaff, A., et al. 2019, MNRAS, 486, 1192
Tully, R. B. 2015, AJ, 149, 171
Tully, R. B., Courtois, H. M., & Sorce, J. G. 2016, AJ, 152, 50
Tully, R. B., Rizzi, L., Shaya, E. J., et al. 2009, AJ, 138, 323
van Dokkum, P., Danieli, S., Cohen, Y., Romanowsky, A. J., & Conroy, C. 2018, ApJL, 864, L18
Veale, M., Ma, C.-P., Greene, J. E., et al. 2018, MNRAS, 473, 5446
Verde, L., Treu, T., & Riess, A. G. 2019, NatAs, 3, 891
Villaume, A., Conroy, C., Johnson, B., et al. 2017, ApJS, 230, 23
Waters, C. Z., Magnier, E. A., Price, P. A., et al. 2020, ApJS, 251, 4
Wong, K. C., Suyu, S. H., Chen, G. C. F., et al. 2020, MNRAS, 498, 1420
Wright, E. L. 2006, PASP, 118, 1711
Yuan, W., Riess, A. G., Macri, L. M., Casertano, S., & Scolnic, D. M. 2019, ApJ, 886, 61
Zaroubi, S., Bernardi, M., da Costa, L. N., et al. 2001, MNRAS, 326, 375